International Journal of Mechanical Sciences 166 (2020) 105243

Contents lists available at ScienceDirect

International Journal of Mechanical Sciences

journal homepage: www.elsevier.com/locate/ijmecsci

Time periodic natural convection heat transfer in a nano-encapsulated phase-change suspension

Ahmad Hajjar[a], S.A.M. Mehryan[b], Mohammad Ghalambaz[c,d,*]

[a] LabECAM, ECAM Lyon, Université de Lyon, Lyon, France
[b] Young Researchers and Elite Club, Yasooj Branch, Islamic Azad University, Yasooj, Iran
[c] Department for Management of Science and Technology Development, Ton Duc Thang University, Ho Chi Minh City, Vietnam
[d] Faculty of Applied Sciences, Ton Duc Thang University, Ho Chi Minh City, Vietnam

ARTICLE INFO

Keywords:
Nano-encapsulated phase change materials (NEPCMs)
Fusion temperature
Time-periodic temperature boundary condition
Natural convection

ABSTRACT

The natural convection of a Nano Encapsulated Phase Change Materials (NEPCMs) suspension in a cavity with a hot wall having a time-periodic temperature is investigated. The top and bottom walls of the enclosure are insulated, the right side wall is kept at a constant temperature of T_c while the left side wall is considered as hot wall and is subjected to a time-periodic temperature. The NEPCM consist of capsules with phase change material PCM in their core. The phase change core of the capsules is covered by a shell. During the fusion or the solidification of the core, the phase change will absorb or release heat in the surrounding, when the temperature is close to the PCM fusion temperature. The partial differential equations governing the flow and heat transfer in the enclosure are formulated in the dimensionless form, and affective key dimensionless numbers and parameters are introduced. The finite element method is used to solve the governing equations. The accuracy of the results is verified by comparison to the benchmark solutions available in the literature. The average Nusselt number in the enclosure, as an indicator of the heat transfer performance, is analyzed. It is shown that the average Nusselt number in the enclosure follows a periodic variation with the same frequency of the temperature of the hot wall and with an amplitude that varies correspondingly with the temperature amplitude. The heat transfer in the cavity is enhanced when a higher fraction ϕ of the NEPCM is used, and a fraction of 5% provides the highest heat transfer. Increasing the volume fraction of nanoparticles from 2.5% to 5% enhanced the average Nusselt number by 21% and the maximum value of Nusselt number by 18.5%. The fusion temperature of nanocapsules is an important parameter affecting the thermal performance of the enclosure, mainly, when the fusion temperature is notably different from cold or hot-wall temperatures.

1. Introduction

Phase change materials (PCM) have been an active research area in recent years, due to their use in thermal storage applications. Such applications include, among others, the thermal performance of buildings [1], domestic air-conditioning systems [2], and electronic devices and space instruments [3]. The main advantage of PCMs is their large latent heat for a relatively small temperature difference and volume change. Heat storage or release occurs at a certain fusion temperature when the PCM undergo melting or solidification, respectively. However, despite the ability of PCMs to store large amounts of energy, these materials are not very efficient in terms of heat transfer due to their low thermal conductivity. Thus, many techniques have been developed to enhance the heat transfer of PCM, such as the use of metallic fins [4,5] or porous media [6–8].

In devices and systems subject to temperature rise or to temperature gradients, like computer chipsets, laser alignment systems, and detectors needing temperature control, internal thermal stresses can develop inside the system due to the disparity of thermal expansion coefficient between different materials. In this context, encapsulation of PCM presents an effective method to enhance the performance of the working fluids and to better control of the system temperature.

Encapsulation consists of using capsules with a shell-core structure, where the core is made of PCM [9]. For instance, Fang et al. [10] used formaldehyde as a shell and n-tetradecane as a core and. Qiu et al. [11] synthesized capsules with n-octadecane as a core encapsulated in MMA-polymer shell. Based on the size of the particles, the terms nano-encapsulation and micro-encapsulation are often used [12,13]. Nano-Encapsulated Phase Change Materials (NEPCMs) dispersed in fluids can, therefore, be considered as nanofluids. It is worth noting that

* Corresponding author.
E-mail addresses: ahmad.hajjar@ecam.fr (A. Hajjar), alal171366244@gmail.com (S.A.M. Mehryan), mohammad.ghalambaz@tdtu.edu.vn (M. Ghalambaz).

https://doi.org/10.1016/j.ijmecsci.2019.105243
Received 26 July 2019; Received in revised form 10 October 2019; Accepted 14 October 2019
Available online 15 October 2019

Nomenclature

Latin letters

a	dimensional temperature amplitude (°C)
A	dimensionless temperature amplitude
Cp	constant pressure specific-heat (J/kg.K)
Cr	ratio of the heat capacity
f	dimensionless frequency
g	gravity constant (m/s^2)
H	size of the enclosure
k	coefficient of thermal conductivity (W/m.K)
Nc	thermal conductivity number
Nu	heat transfer characteristic (Nusselt number)
Nv	dynamic viscosity number
p	dynamic pressure inside the fluid domain (Pa)
P	dimensionless dynamic pressure inside the fluid domain
Pr	Prandtl number of the PCM ($\mu_f/(\rho_f\alpha_f)$)
Ra	Rayleigh number of the PCM ($g\rho_f\beta_f(T_h\text{-}T_c)H^3/(\alpha_f\mu_f)$)
S	the non-dimensional fusion function
Ste	Stefan number
T	temperature (°C)
TMr	phase-change temperature range $T_{Mr} = T_2 - T_1$ (°C)
u	dimensional x-velocity component (m/s)
U	dimensionless x-velocity component
v	dimensional y-velocity component (m/s)
V	dimensionless y-velocity component
x, y	Cartesian space
X, Y	non-dimensional Cartesian space
ι	ratio of the weight of nanoparticles' PCM-core to the shell

Greek symbols

μ	melt dynamic viscosity (kg s/m)
α	thermal diffusivity (m^2/s)
β	the coefficient of volumetric thermal expansion (1/K)
δ	dimensionless range of fusion temperature
τ	dimensionless time
τ_p	dimensionless time period
θ	dimensionless temperature
λ	the heat capacity ratio of nanoparticles to the host fluid
σ	dimensional rectangular function
Ξ	dimensionless rectangular function
ω	temperature frequency
ρ	density (kg/m^3)
ϕ	nanoparticles's volume fraction
ψ	dimensionless stream-function

Subscript

b	bulk properties for the NEPCM nanofluid
c	cold wall
co	PCM core of nanoparticles
f	host fluid
fu	phase change property at fusion temperature
h	hot wall
p	NEPCM nanoparticles
sh	shell of NEPCM particle

many studies considered the addition of nanoparticles to PCM for heat transfer enhancement [1,14,15]. In the presence of such nano-additives, the acronym NEPCM means Nano-Enhanced Phase Change Materials [14,16–18], which is different from the technique considered in the present study.

Natural convection of nanofluids, i.e., fluids comprising suspensions of nanoparticles, in cavities and enclosures have been widely investigated. Suspensions of uniform solid particles without phase change in cavities with different configurations, such as wavy walled cavities [19,20], cavities with hot wall obstacles [21] and porous enclosures [22,23] have been considered. Other studies addressed the effects of magnetic fields [24] and conjugate heat transfer [25] on the natural convection of the nanofluid in the enclosure. Taking phase change of NEPCM into account, most of the studies focused on forced convection in channels or tubes. For instance, [26] performed a numerical study of the heat transfer enhancement in microtube heat sinks by PCM encapsulation and concluded that while the presence of the NEPCM substantially improved the fluid cooling power, it leads to a significant pressure drop in the tube. Seyf et al. [27] investigated the flow and heat transfer of a slurry of nano-encapsulated octadecane past a square cylinder numerically and found a remarkable enhancement of the heat transfer characteristics of the slurry with respect to the base fluid. Ho et al. [28] conducted experiments to investigate the effect of using water-based microencapsulated PCM on heat transfer in a minichannel. They observed that heat transfer can be enhanced or deteriorate by the presence of the PCM capsules depending on various parameters like the flow rate and the latent-sensible heat ratio. Other experiments [29,30] used Alumina nanoparticles and/or slurries of microencapsulated PCM in circular tubes [29] and minichannels [30]. Their results also indicated that heat transfer performance is affected by different parameters, such as the flow rate and the heating location.

On the other hand, works dealing with the natural convection of NEPCM suspensions have been very limited. In a recent study [31], we investigated the steady natural convective flow of NEPCM in a square cavity with two differentially-heated isothermal vertical walls and found that the heat transfer enhancement depends greatly on the fusion temperature of the NEPCM. In practice, it is very possible that the temperature of the walls fluctuates with time and, thus, the assumption of isothermal walls cannot be valid. The presence of an unsteady time-periodic heat transfer can contribute to the thermal charging/discharging capability of NEPCMs and provide a different trend of behavior rather than the steady-state case which was investigated in [31]. The present research aims to examine the case of a cavity with a time-dependent temperature boundary condition. For the sake of simplicity, the temperature is assumed to be time-periodic.

2. Problem physics

As demonstrated in Fig. 1, the geometry considered is a 2D square enclosure, which is occupied by a water-NEPCM suspension. The components of NEPCM are polyurethane (PU) and nonadecane as the shell and the core. As indicated in Fig. 1, the left wall of the enclosure is heated at a higher time-periodic temperature with an average temperature of T_h. The opposite side is maintained at a lower temperature of T_c. The other walls of the enclosure are perfectly insulated. It is assumed that the suspension is incompressible, and its flow is laminar. There are no thermal and hydro-dynamic slips between the host fluid and uniformly dispersed PU- nonadecane particles.

Table 1 lists thermo-physical properties of the components of the suspension. The fusion temperature and latent heat of the NEPCMs core are about 32 °C and 211 kJ/kg, respectively [32].

2.1. The formulation

According to the foregoing assumptions, the equations modeling thermal and hydrodynamic behavior of a suspension have been listed below [31]:

Conservation of mass:

$$\frac{\partial u}{\partial x} + \frac{\partial v}{\partial y} = 0 \tag{1}$$

Conservation of momentum:

$$\rho_b\left(\frac{\partial u}{\partial t} + u\frac{\partial u}{\partial x} + v\frac{\partial u}{\partial y}\right) = -\frac{\partial p}{\partial x} + \mu_b\left(\frac{\partial^2 u}{\partial x^2} + \frac{\partial^2 u}{\partial y^2}\right) \tag{2a}$$

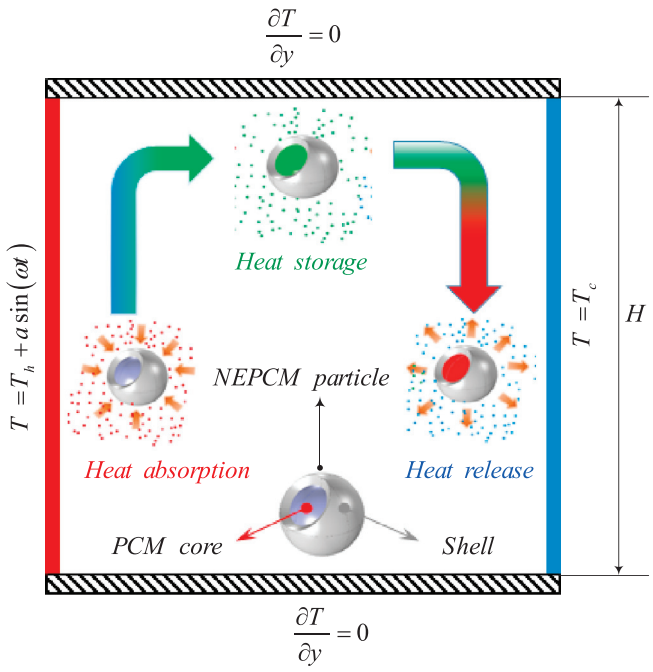

Fig. 1. Schematic configuration of the considered geometry.

$$\rho_b\left(\frac{\partial v}{\partial t}+u\frac{\partial v}{\partial x}+v\frac{\partial v}{\partial y}\right)=-\frac{\partial p}{\partial y}+\mu_b\left(\frac{\partial^2 v}{\partial x^2}+\frac{\partial^2 v}{\partial y^2}\right)+g\rho_b\beta_b(T-T_c) \quad (2b)$$

Conservation of energy:

$$(\rho C_p)_b\left(\frac{\partial T}{\partial t}+u\frac{\partial T}{\partial x}+v\frac{\partial T}{\partial y}\right)=k_b\left(\frac{\partial^2 T}{\partial x^2}+\frac{\partial^2 T}{\partial y^2}\right) \quad (3)$$

Regarding the no-slip condition on the walls and the schematic configuration, the boundary conditions are defined as:

$$\forall x,y\,|\,x=0,0\le y\le H\Rightarrow u=v=0,T=T_h+a\sin(\omega t) \quad (4a)$$

$$\forall x,y\,|\,x=H,0\le y\le H\Rightarrow u=v=0,T=T_c \quad (4b)$$

$$\forall x,y\,\left|\begin{array}{l} y=0,0\le x\le H\ \Rightarrow u=v=0,\frac{\partial T}{\partial y}=0\\ y=H,0\le x\le H\ \Rightarrow u=v=0,\frac{\partial T}{\partial y}=0\end{array}\right. \quad (4c)$$

The density of the suspension is written as a weighted function of the densities of the host fluid and NEPCM dispersed particles [9,34]:

$$\rho_b=(1-\phi)\rho_f+\phi\rho_p \quad (5a)$$

$$\rho_p=\frac{(1+\imath)\rho_{co}\rho_{sh}}{\rho_{sh}+\imath\rho_{co}} \quad (5b)$$

$\imath$ is the weight ratio of the core to the shell, and it is about $\imath\sim0.447$ [32]. It is worth mentioning that the core density is an average of the densities of the core liquid and solid phases. The specific heat capacity of the suspension can be calculated as [34,35]:

$$C_{p,b}=\frac{(1-\phi)\rho_f C_{p,f}+\phi\rho_p C_{p,p}}{\rho_b} \quad (6)$$

For the process with no phase change, $C_{p,p}$ is measured by the following relation:

$$C_{p,p}=\frac{(C_{p,co}+\imath C_{p,sh})\rho_{co}\rho_{sh}}{(\rho_{sh}+\imath\rho_{co})\rho_p} \quad (7)$$

A sinusoidal profile, which considers the latent heat of the core, is applied to model the specific heat capacity of the NEPCM particles [31]:

$$C_{p,p}=C_{p,co}+\left\{\frac{\pi}{2}\cdot\left(\frac{h_{sf}}{T_{Mr}}-C_{p,co}\right)\cdot\sin\left(\pi\frac{T-T_0}{T_{Mr}}\right)\right\}\sigma$$
$$\sigma=\begin{cases}0 & T<T_0\\ 1 & T_0<T<T_1\\ 0 & T>T_1\end{cases}\left|\begin{array}{l}T_0=T_{fu}-T_{Mr}/2\\ T_1=T_{fu}+T_{Mr}/2\end{array}\right. \quad (8)$$

The thermal volume expansion coefficient of the suspension is as follow [35]:

$$\beta_b=(1-\phi)\beta_f+\phi\beta_p \quad (9)$$

The linear relations presented below are used to assess the thermal conductivity and dynamic viscosity of the suspension [14,36]:

$$\frac{k_b}{k_f}=1+Nc\phi \quad (10a)$$

$$\frac{\mu_b}{\mu_f}=1+Nv\phi \quad (10b)$$

It is worth noting that the relations of Eq. (10) are only acceptable for diluted nanofluids with $\phi<5\%$.

2.2. Non-dimensional form of governing equations

To dimensionalize the mentioned governing equations as well as the imposed boundary conditions, the following variations are utilized:

$$X=\frac{x}{H},\quad Y=\frac{y}{H},\quad U=\frac{uH}{\alpha_f},\quad V=\frac{vH}{\alpha_f},$$
$$P=\frac{pH^2}{\rho_f\alpha_f^2},\quad \theta=\frac{T-T_c}{T_h-T_c},\quad \tau=\frac{\alpha_f t}{H^2},\quad A=\frac{a}{T_h-T_c} \quad (11)$$

Hence, we then have:

$$\frac{\partial U}{\partial X}+\frac{\partial V}{\partial Y}=0 \quad (12)$$

$$\left(\frac{\rho_b}{\rho_f}\right)\left(\frac{\partial U}{\partial\tau}+U\frac{\partial U}{\partial X}+V\frac{\partial U}{\partial Y}\right)=-\frac{\partial P}{\partial X}+Pr\left(\frac{\mu_b}{\mu_f}\right)\left(\frac{\partial^2 U}{\partial X^2}+\frac{\partial^2 U}{\partial Y^2}\right) \quad (13)$$

$$\left(\frac{\rho_b}{\rho_f}\right)\left(\frac{\partial V}{\partial\tau}+U\frac{\partial V}{\partial X}+V\frac{\partial V}{\partial Y}\right)=-\frac{\partial P}{\partial Y}+Pr\left(\frac{\mu_b}{\mu_f}\right)\left(\frac{\partial^2 V}{\partial X^2}+\frac{\partial^2 V}{\partial Y^2}\right)+Ra\cdot Pr\left(\frac{\beta_b}{\beta_f}\right)\left(\frac{\rho_b}{\rho_f}\right)\theta \quad (14)$$

which

$$Ra=\frac{g\rho_f\beta_f(T_h-T_c)H^3}{\alpha_f\mu_f},\quad Pr=\frac{\mu_f}{\rho_f\alpha_f} \quad (15)$$

Table 1
Thermophysical properties of the involved material in the problem [32,33].

	k (W/m.K)	ρ (kg/m^3)	C_p (KJ/kg.K)	β (K^{-1})	μ (kg/m. s)
Host fluid	0.613	997.1	4179	21×10^{-5}	8.9×10^{-4}
PU	—	786	1317.7	17.28×10^{-5}	—
Nonadecane	—	721	2037		—

$$Cr\left(\frac{\partial\theta}{\partial\tau}+U\frac{\partial\theta}{\partial X}+V\frac{\partial\theta}{\partial Y}\right)=\left(\frac{k_b}{k_f}\right)\left(\frac{\partial^2\theta}{\partial X^2}+\frac{\partial^2\theta}{\partial Y^2}\right) \tag{16}$$

where

$$Cr=\frac{\left(\rho C_p\right)_b}{\left(\rho C_p\right)_f}=(1-\phi)+\phi\lambda+\frac{\phi}{\delta\, Ste}S \tag{17}$$

Herein, Cr is the ratio of the suspension heat capacity to the sensible heat capacity of the host fluid. As detailed mentioned, the suspension heat capacity consists of the latent and sensible heats. Furthermore, the sensible heat capacity ratio λ, the dimensionless range of fusion temperature δ, and Stefan number Ste can respectively be defined as follows:

$$\lambda=\frac{\left(C_{p,co}+\imath C_{p,sh}\right)\rho_{co}\rho_{sh}}{\left(\rho C_p\right)_f\left(\rho_{sh}+\imath\rho_{co}\right)},\quad \delta=\frac{T_{Mr}}{\Delta T},$$
$$Ste=\frac{\left(\rho C_p\right)_f\Delta T\left(\rho_{sh}+\imath\rho_{co}\right)}{\alpha_f\left(h_{sf}\rho_{co}\rho_{sh}\right)} \tag{18}$$

Also,

$$\left(\frac{\rho_b}{\rho_f}\right)=(1-\phi)+\phi\left(\frac{\rho_p}{\rho_f}\right),$$
$$\left(\frac{\beta_b}{\beta_f}\right)=(1-\phi)+\phi\left(\frac{\beta_p}{\beta_f}\right) \tag{19}$$

It is assumed that the thermal expansion of the NEPCM particles is the same as the base fluid, and hence, $\beta_b/\beta_f\sim 1$. S, known as the dimensionless fusion function, is equal to:

$$S=\frac{\pi}{2}\sin\left(\frac{\pi}{\delta}\left(\theta-\theta_{fu}+\delta/2\right)\right)\Xi$$
$$\Xi=\begin{cases}0 & \theta<\theta_{fu}-\delta/2\\ 1 & \theta_{fu}-\delta/2<\theta<\theta_{fu}+\delta/2\\ 0 & \theta>\theta_{fu}+\delta/2\end{cases}\Bigg|\begin{matrix}\theta_{fu}=\dfrac{\left(T_{fu}-T_c\right)}{\Delta T}\\ \Delta T=T_h-T_c\end{matrix} \tag{20}$$

Eventually, the forms of boundary conditions in the non-dimensional coordinates can be obtained as:

$$\forall X,Y|X=0,0\le Y\le 1\ \Rightarrow U=V=0,\theta=1+A\sin(f\tau) \tag{21a}$$

$$\forall X,Y|X=1,0\le Y\le 1\ \Rightarrow U=V=0,\theta=0 \tag{21b}$$

$$\forall X,Y\begin{cases}Y=0,0\le X\le 1\ \Rightarrow U=V=0,\dfrac{\partial\theta}{\partial Y}=0\\ Y=1,0\le X\le 1\ \Rightarrow U=V=0,\dfrac{\partial\theta}{\partial Y}=0\end{cases} \tag{21c}$$

where f is the non-dimensionalized temperature frequency so that $f=\omega L^2/\alpha_f$. To display the velocity field, stream function ψ is defined as follow:

$$\frac{\partial^2\psi}{\partial X^2}+\frac{\partial^2\psi}{\partial Y^2}=-\left(\frac{\partial V}{\partial X}-\frac{\partial U}{\partial Y}\right) \tag{22}$$

Since the velocity vectors are tangent to the streamlines, the walls can be considered as streamlines with the value of zero.

2.3. Heat transfer rate

The rate of heat transfer through the hot wall at a specific time τ is obtained by the relation given below:

$$Nu_{a,\tau}=-(1+Nc\phi)\int_0^1\left(\frac{\partial\theta}{\partial X}\right)_{Y=0}dY \tag{23}$$

The time-averaged Nusselt number over one period τ_p ($\tau_p=2\pi/f$) is defined as:

$$Nu_a=\frac{1}{\tau_p}\int_{n\tau_p}^{(n+1)\tau_p}\int_0^1 Nu_{a,\tau}\,dY\,d\tau \tag{24}$$

In order to study the effects of dispersing NEPCMs in the host fluid, the Normalized average Nusselt number ($NNu_{\phi=0}$) is studied as:

$$NNu_{\phi=0}=\frac{Nu_a}{Nu_a\big|_{\phi=0}} \tag{25}$$

Also, in order to study the effect of the core-phase change of the nanoparticles on the heat transfer rate, the Nusselt number can be normalized based on a process with no phase change. Therefore, in this case, the Normalized Nusselt number ($NNu_{Ste\to\infty}$) can be introduced as:

$$NNu_{Ste\to\infty}=\frac{Nu_a}{Nu_a\big|_{Ste\to\infty}} \tag{26}$$

3. Numerical approach, grid test, and verification

Highly non-linear equations describing the flow and temperature fields are solved by using the finite element method. The utilized method can be found in details in [37]. The computational domain is discretized using a structured mesh consisting of $N\times N$ rectangular elements. The mesh is refined near the walls and gradually coarsened towards the domain center. The selection of an adequate time step is very important in phase change heat transfer. Hence, in the present study, the time step is controlled automatically using a free time-step Backward Differentiation Formula (BDF) [38]. A grid independence test was performed to determine the optimal number of elements for the numerical computations. The test was done for $\phi=0.05$, $Ste=0.2$, $Ra=10^6$, $\theta_f=0.25$, $f=0.05$, and $A=1$. Three grids were considered: 50×50, 100×100 and 150×150. The variation of the non-dimensional horizontal velocity U and the non-dimensional temperature θ along the central line of the domain ($X=0.5$), at $\tau=2\tau_p$, for the three grids is plotted in Fig. 2. It is shown that varying the grid size has minimal impact on the results. It was then decided to use a 100×100 grid in the computations, as it shows a good compromise between good numerical precision and low computational cost. Besides, to verify the numerical model for suspension simulations comprising NEPCMs particles, initial calculations are done and evaluated with the works conducted in [39–41].

Turan et al. [39] investigated the steady natural convection in a cavity when the top and bottom walls were insulated, and the side walls were at a constant temperature. The right and the left walls were at hot and cold temperatures, respectively. For a case of Newtonian fluid with $Pr=1000$ and $Ra=10^5$, a comparison between the isotherms of the present study and those of [39] is reported in Fig. 3. As seen, the results are in excellent agreement.

As a transient heat transfer case, a comparison with the results of Kalabin et al. [41] in performed in Fig. 4. Kalabin et al. [41] studied an unsteady natural convection heat transfer in a square cavity with the adiabatic horizontal walls. A time-periodic temperature varying by sinusoidal law about the average value of T_c was applied to the left vertical wall. The other sidewall was at an isothermal temperature of T_c.

The average Nusselt number of the current study with that given in [41] is compared when $Ra=2\times 10^5$, $Pr=1$, and $f=20\pi$. As shown in Fig. 4, the results of the current work are in good agreement with Kalabin et al. [41]. In another verification, a comparison of the average Nusselt number for different values of the volume fraction ϕ, obtained by the present work and the solution of Kahveci et al. [40] is carried out. The left and right of the enclosure investigated by Kahveci et al. [40] were maintained at the higher and lower temperatures, while the

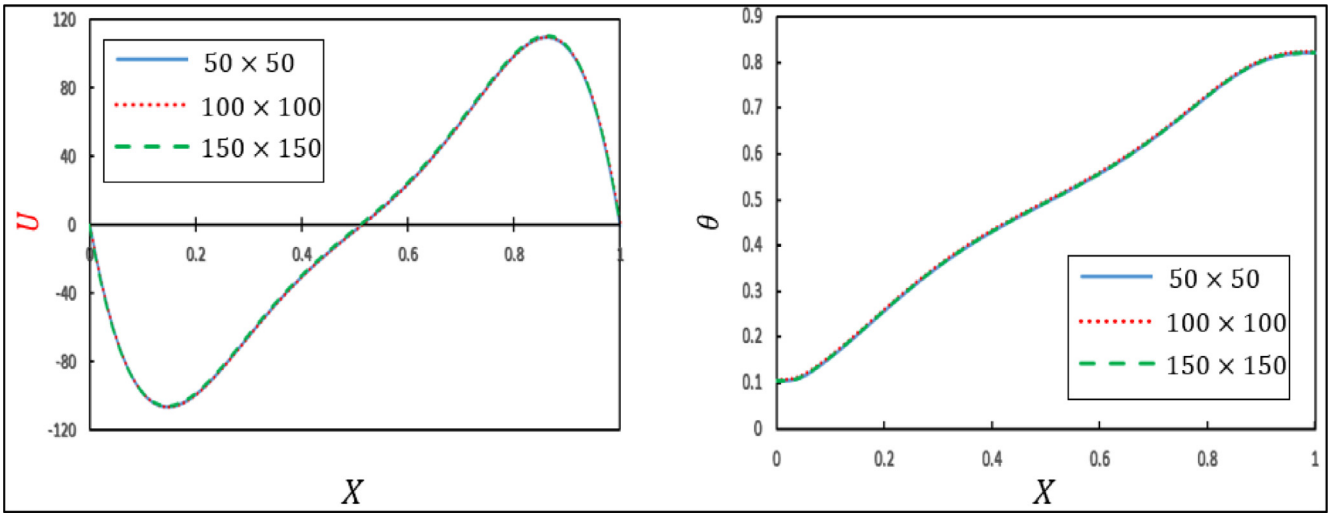

Fig. 2. Profiles of diemensionless velocity U and temperature θ for different grids at $\tau = 2\tau_p$, and for $\phi = 0.05$, $Ste = 0.2$, $Ra = 10^6$, $\theta_f = 0.25$, $f = 0.05$, and $A = 1$.

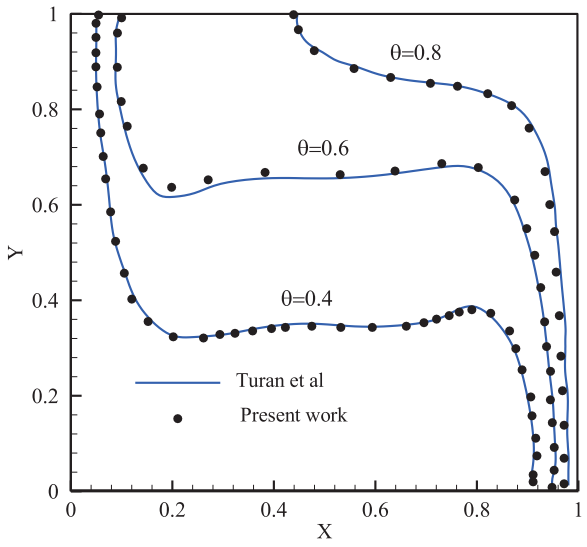

Fig. 3. comparison of the temperature field from work conducted by Turan et al. [39] and the present prediction.

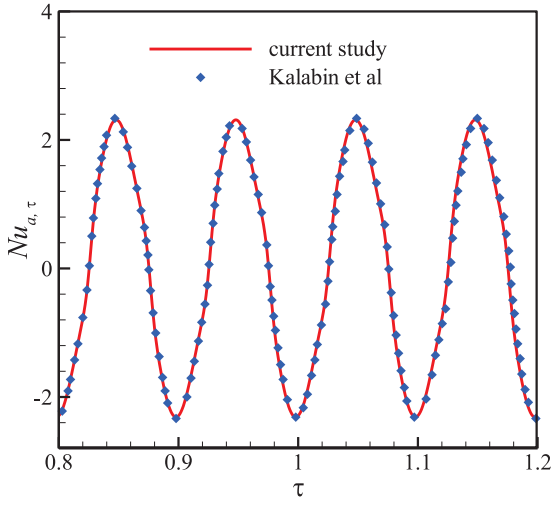

Fig. 4. Nusselt number reported by Kalabin et al. [41] and that of the utilized numerical approach in the current study.

Table 2
The average Nusselt numbers of the present investigation and Kahveci et al. [40] for $Ra = 10^6$.

	$\phi = 0$	$\phi = 0.05$	$\phi = 0.1$	$\phi = 0.15$	$\phi = 0.2$
Present study	9.20	9.76	10.3	10.8	11.2
Kahveci et al	9.23	9.783	10.297	10.771	11.206

other walls were perfectly insulated. The thermal conductivity and dynamic viscosity numbers for the comparison are 3.3 and 2.88, respectively. As found clearly from Table 2, the outcomes of the employed code match the outcomes presented by Kahveci et al. [40]. According to the conducted verifications, the provided code can confidently be used to reach the correct and accurate results.

4. Results and discussion

In this work, the thermal and dynamic behavior of a suspension comprising NEPCMs particles in a square cavity with a time-varying hot wall temperature is investigated. The non-dimensional parameters are the particles' volume fraction ϕ, the density ratio ρ_p/ρ_f, the heat capacity ratio λ, the Stefan number Ste, the fusion temperature of the particles' core θ_f, the thermal conductivity number Nc, the dynamic viscosity number Nv, the Rayleigh number Ra and the Prandtl number Pr. As the suspension is dilute, the volume fraction ϕ should be less than 5%. Based on the experimental data presented by Barlak et al. [32] for a water-NEPCM suspension, the thermal conductivity Nc and dynamic viscosity Nv numbers are respectively calculated as $Nc = 23.8$ and $Nv = 12.5$. Also, the sensible heat capacity ratio λ reported by Barlak et al. [32] is 0.32. Here, the numerical investigation is performed for the alterable parameters consisting of the Rayleigh number $10^5 \le Ra \le 10^7$, Stefan number $0.2 \le Ste \le \infty$, non-dimensional fusion temperature $0.05 \le \theta_f \le 1$, dimensionless frequency $0.01\pi \le f \le \pi$, amplitude $0.0 \le A \le 1$, and the volume fraction of the NEPCM particles $0.0 \le \phi \le 5\%$. The Prandtl number is selected as $Pr = 6.2$, as it is the value regularly used for water. The Rayleigh number can be varied between 10^5 and 10^7, where high values indicate a heat transfer dominated by natural convection. The temperature of the cold wall is fixed at $\theta_c = 0$, while that of the hot wall is following the periodic variation $\theta = 1 + Asin(f\tau)$.

The default values of the main parameters are $\phi = 0.05$, $Ste = 0.2$, $Ra = 10^6$, $\theta_f = 0.25$, $\delta = 0.05$, $f = 0.05$, and $A = 1$. In the following, unless stated otherwise, the results are reported for these default values. In order to investigate the effect of a specific parameter on the heat transfer

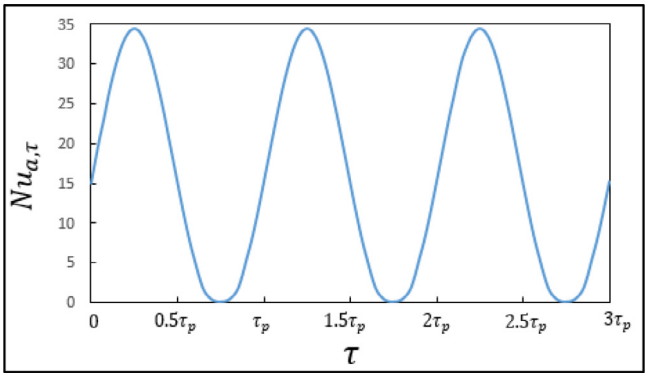

Fig. 5. Variation of the Nusselt number $Nu_{a,\tau}$ as a function of time for the default parameters values.

inside the cavity, its value will be varied in a defined range, while the other parameters will keep their default values.

Fig. 5 represents the variation of the Nusselt number at the hot wall $Nu_{a,\tau}$ as a function of time, when all the parameters are given their default values. Like the temperature of the hot wall, $Nu_{a,\tau}$ presents a periodic variation, with the maximum being at $\tau = 0, 0.25\tau_p, 1.25\tau_p$ and $2.25\tau_p$, which correspond to the instants at which the temperature of the hot wall is maximum $\theta = 1 + A$. For $\tau = 0, 0.75\tau_p, 2.25\tau_p$, $Nu_{a,\tau} = 0$ as the temperature of the hot wall is equal to that of the cold wall $\theta = 1 - A = \theta_c$, and therefore, no heat is transferred through the hot wall. The heat transfer rate in the cavity will thus be oscillating with repeated high heat transfer periods followed by no transfer periods.

In order to investigate the effects of the frequency and the amplitude of the hot wall temperature on the heat transfer in the cavity, $Nu_{a,\tau}$ is plotted as a function of time for different values of f (shown in Fig. 6) and A (shown in Fig. 7). It is clear that the Nusselt number in the case of a constant hot wall temperature ($f = 0$ or $A = 0$) is equal to the average Nusselt number Nu_a in the case where $f \neq 0$ and $A \neq 0$. Increasing the frequency of the oscillations does not have any effect on the amplitude of $Nu_{a,\tau}$. However, it confirms that the frequency of variation of $Nu_{a,\tau}$ is always equal to that of the hot wall temperature. On the other side, increasing A does not change Nu_a but it increases the amplitude of $Nu_{a,\tau}$. These results indicate that the frequency of variation of the heat transfer intensity in the cavity always follows the frequency of the time-periodic temperature. A temperature with a higher amplitude will lead to an increased heat transfer when the temperature is maximum. It is worth noting that for $A = 1.5$ (as shown in Fig. 6), at $\tau = 2.75\ \tau_p$, $Nu_{a,\tau}$ has a negative value. In fact, the temperature of the hot wall at this instant is equal to $\theta = -0.5$, which is lower than θ_c, thus leading to a negative heat transfer rate as the hot wall will behave as the cold one and vice versa. Anyway, in all the cases, the average value Nu_a will always be the same.

The variation of $Nu_{a,\tau}$ as a function of time for different values of the nanoparticles (NEPCMs) volume fraction ϕ is illustrated in Fig. 8a. It is shown that a higher value of ϕ increases the average Nusselt number Nu_a as well as the amplitude of $Nu_{a,\tau}$. In the case of a pure fluid ($\phi = 0$), $Nu_{a,\tau}$ is varying periodically around the average value $Nu_a = 9.19$, with a maximum of 22.36. Increasing ϕ to 0.025 and 0.05 increases Nu_a respectively to 12.45 and 15.15 (21% enhancement) and the maximum values of Nusselt to 29.12 and 34.51 (18.5% enhancement). An increase of the volume fraction of the NEPCM would lead to higher latent heat storage and consequently would enhance the heat transfer in the enclosure. Fig. 8.b shows that the Normalized average Nusselt number $NNu_{\varphi=0}$ reaches its maximal value for $\phi = 0.05$. This means that the optimal value of the NEPCM particles volume fraction is 5%, as it is the maximum value in the range that corresponds to dilute suspensions, thus respecting the assumptions of the study.

Fig. 9 shows the variation of $Nu_{a,\tau}$ as a function of time for $Ra = 10^5$, 10^6 and 10^7. It is shown that increasing the value of Ra increases substantially the amplitude of $Nu_{a,\tau}$ and the average Nusselt number Nu_a. Indeed, Ra expresses heat transfer in natural convection, and increasing its magnitude will thus enhance the heat transfer rate in the enclosure.

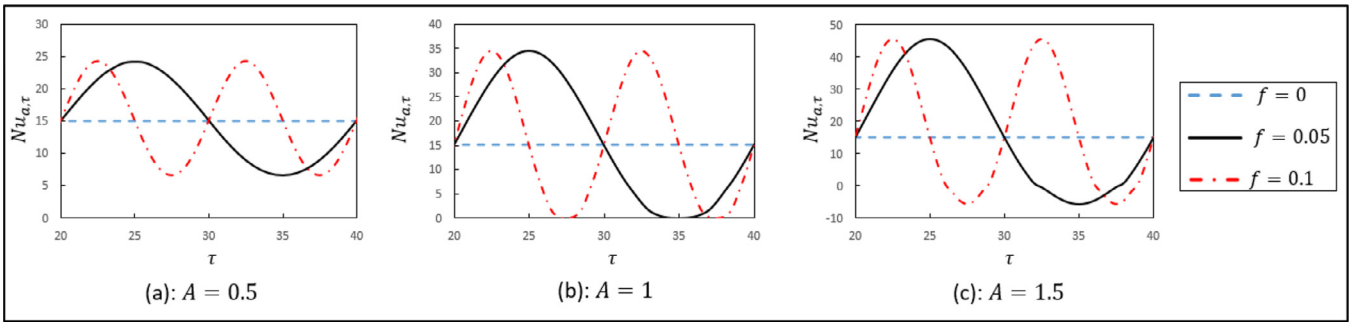

Fig. 6. Variation of $Nu_{a,\tau}$ as a function of time for $A = 0.5$, $A = 1$ and $A = 1.5$, and for various values of f.

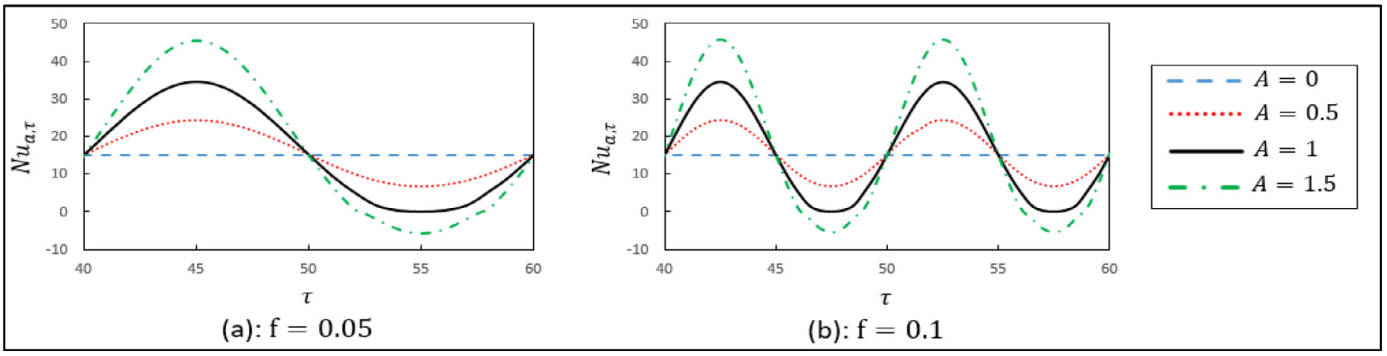

Fig. 7. Variation of $Nu_{a,\tau}$ as a function of time for $f = 0.05$ and $f = 0.1$ and for various values of A.

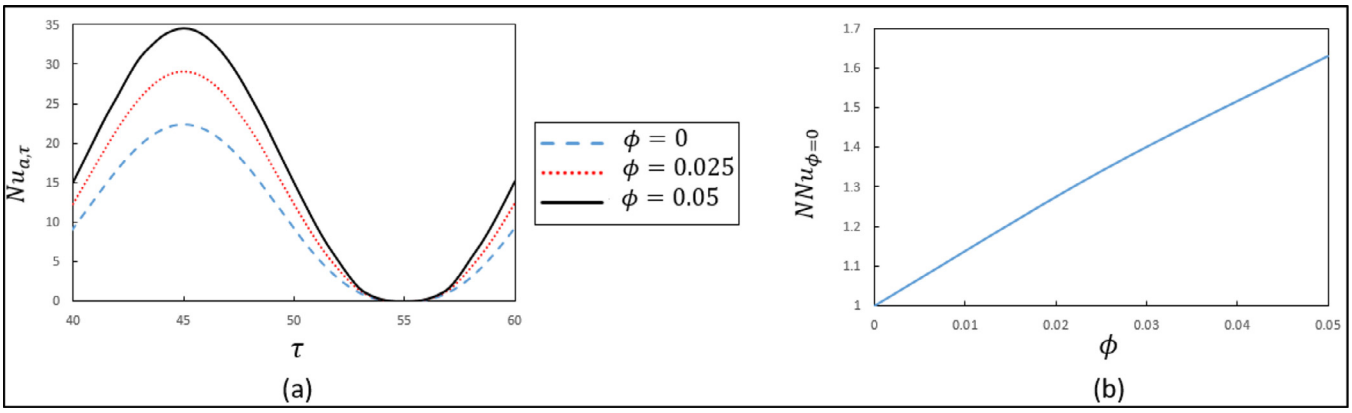

Fig. 8. (a) Time variation of $Nu_{a,\tau}$ for different values of the volume concentration ϕ. (b) Variation of the Normalized average Nusselt number $NNu_{\phi=0}$ as a function of ϕ.

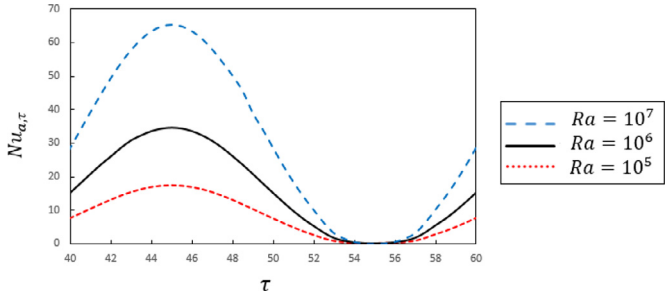

Fig. 9. Time variation of $Nu_{a,\tau}$ as a function of time for different values of Ra.

The impact of Stefan number Ste and the fusion temperature θ_f and on the rate of heat transfer is depicted in Fig. 10. For all the values of Ste, varying θ_f in the range [0, 0.75] shows that increasing θ_f changes the magnitude of $Nu_{a,\tau}$ slightly. To further illustrate the effect of θ_f and Ste, the variation of $Nu_{a,\tau}$ as a function of θ_f for different values of Ste is plotted in Fig. 11. It should be noted that a decrease of Ste indicates a rise of the PCM core latent heat, and thus, an increase of the heat storage of the NEPCM particles.

The case $Ste \to \infty$ is also plotted to emphasize the case with no phase change. First, it is shown that when Ste decreases, $Nu_{a,\tau}$ increases. This results in a rise in the heat transfer rate in the cavity. In fact, decreasing Ste indicates an increase of the latent heat of the PCM and consequently rises the heat absorbed or released during the phase change process of the particles core. This leads to an enhancement of the heat transfer due to the presence of the NEPCM, translated by the increase of $Nu_{a,\tau}$. For $\tau = 2\tau_p$, at which the temperature of the hot wall is $\theta = 1$, the variation of $Nu_{a,\tau}$ represents a symmetry around $\theta_f = 0.5$. This is explained by the symmetry of the geometry and the boundary conditions. This symmetry is not present for $\tau = 2.25\tau_p$, for which the hot wall temperature is $\theta = 2$. However, one would expect a symmetry around $\theta_f = 1$ if the variation of

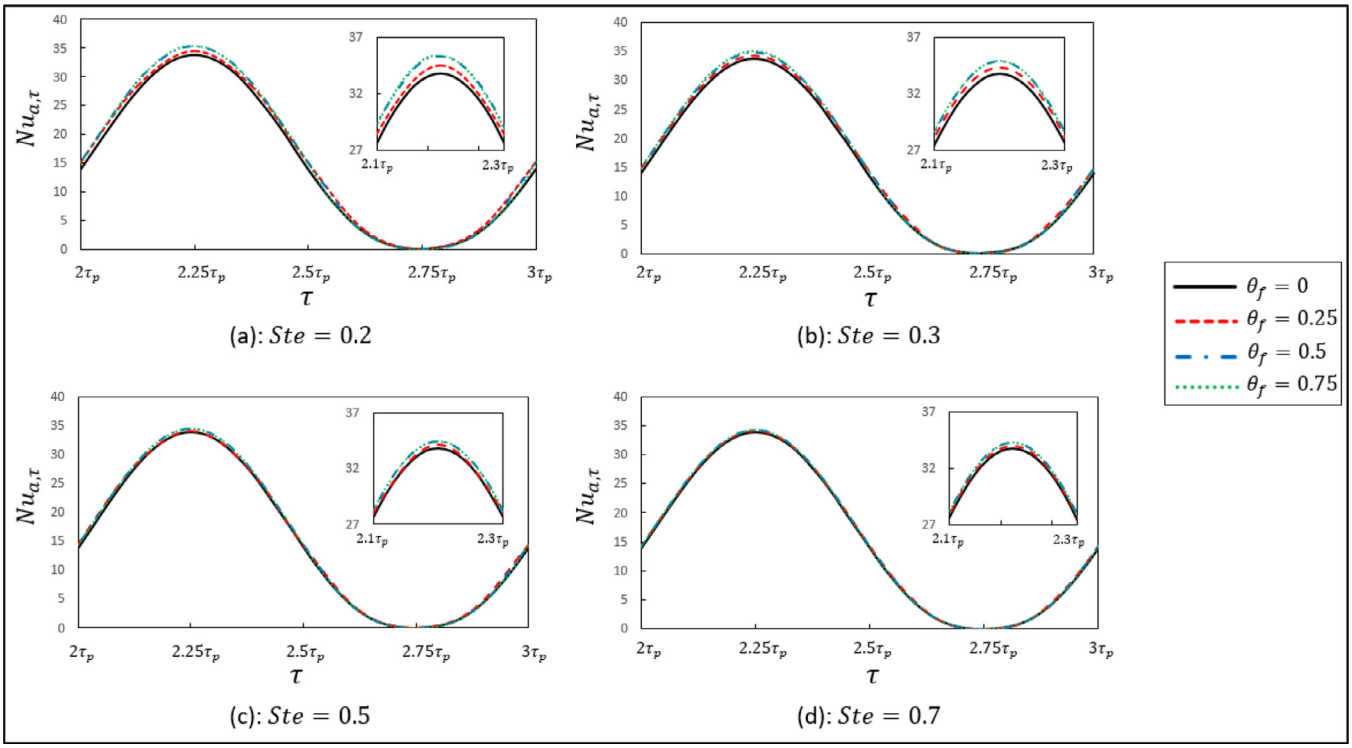

Fig. 10. Time variation of $Nu_{a,\tau}$ as a function of time for different values of θ_f and Ste.

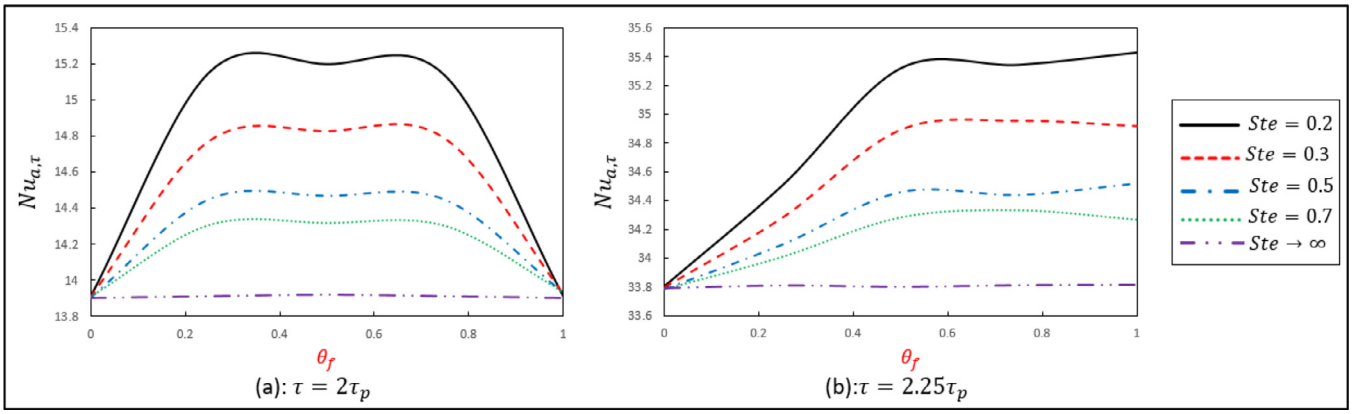

Fig. 11. Variation of $Nu_{a,\tau}$ as a function of θ_f for different values of *Ste*.

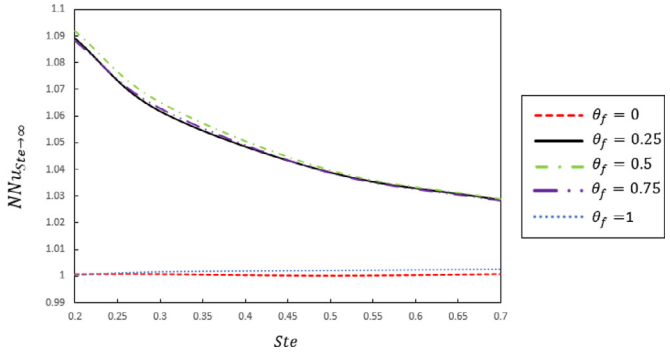

Fig. 12. Variation of $NNu_{Ste\to\infty}$ as a function of Ste for different values of θ_f.

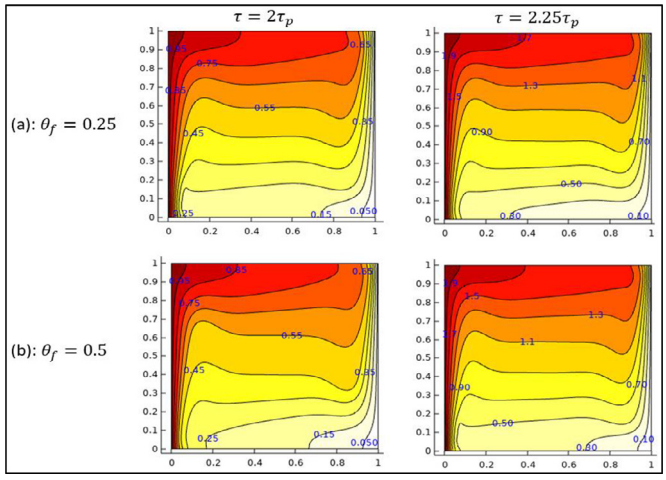

Fig. 13. Isotherm contours for $\theta_f = 0.25$ and $\theta_f = 0.5$.

$Nu_{a,\tau}$ was plotted for θ_f in the range 0–2. In all cases, the heat transfer will be minimum when the fusion temperature θ_f is close to the temperature of the cold wall θ_c or to the maximum temperature of the hot wall θ_{max}. Indeed, the temperature at any point inside the cavity is lower than the hot wall temperature and higher than that of the cold wall. As the phase change of the NEPCM core occurs when the surrounding temperature is very close to θ_f, having a fusion temperature equal to the hot or cold wall temperature means that the phase change of the core inside the cavity is negligible and, therefore, the contribution of the NEPCM to the heat transfer enhancement is insignificant. On the other hand, the heat transfer enhancement is optimal when θ_f is comprised in the interval $[0.25\theta_{max}, 0.75\theta_{max}]$. When $Ste \to \infty$, $Nu_{a,\tau}$ does not vary as no phase change is occurring. The Normalized Nusselt number $NNu_{Ste\to\infty}$ is plotted as a function of *Ste* for different values of θ_f in Fig. 12. It is shown that when the fusion temperature θ_f is close to the temperature of one of the walls, the value of $NNu_{Ste\to\infty}$ remains equal to 1. When θ_f deviates from the walls temperature, $NNu_{Ste\to\infty}$ increases, mostly for small values of *Ste*. This result confirms the fact that the phase change of the PCM cores is an essential factor in heat transfer enhancement. Nonetheless, the phase change of NEPMCs is only effective when the fusion temperature is close to the temperature of the walls, and the value of *Ste* should be kept small.

Figs. 13 and 14 show respectively the isotherm and the heat capacity ratio (*Cr*) contours for $\theta_f = 0.25$ and $\theta_f = 0.5$. At $\tau = 2\tau_p$, the isotherm $\theta_f = 0.25$ starts as a vertical line near the cold wall, then moves in a horizontal direction towards the hot wall where it moves vertically towards the bottom of the hot wall. The isotherm $\theta = 0.5$ follows a very similar variation, but it starts further from the cold wall and ends closer to the hot wall, while its horizontal part is directed towards the center. It is clear that the pattern of the isotherms is slightly affected by the fusion temperature θ_f. However, as the melting and solidification of the NEPCM core occurs when the temperature is close to θ_f, this means that increasing θ_f would move the zone of the phase change towards the center of the cavity and closer to the hot wall. This observation is confirmed by looking at the heat capacity ratio *Cr* depicted in Fig. 14, where the yellow ribbon-shaped zone represents the phase change region. At $\tau = 2.25\tau_p$, the isotherm $\theta = 0.25$ starts at the top of the cold wall with a prolongation in the vicinity of the bottom wall. The shape of the isotherm $\theta = 0.5$ is similar to the case $\tau = 2\tau_p$. The pattern of the isotherm contours is also not affected by the variation of θ_f. Nonetheless, compared to the case $\tau = 2\tau_p$, the contours move towards the bottom wall, due to the fact that the temperature of the hot wall has doubled. In the two cases, the zone of phase change moves upwards when θ_f is increased. Moreover, the ribbon-shaped zone of *Cr* is always wider in the center of the cavity, since the temperature gradients are larger near the walls. In all cases, the maximum value of *Cr* is 8.82.

5. Summary and conclusion

Natural convective flow and heat transfer of a dilute NEPCM suspension in a cavity with time-periodic temperature boundary condition are investigated. An adiabatic boundary condition is imposed on the top and bottom walls, while one of the side walls is kept at a constant temperature and considered as a cold wall. The temperature of the hot wall oscillating around a mean value higher than the temperature of the cold wall. Due to temperature difference, a buoyancy-driven flow is created in the cavity. The equations governing flow and heat transfer inside the cavity are formulated in the dimensionless form. The latent

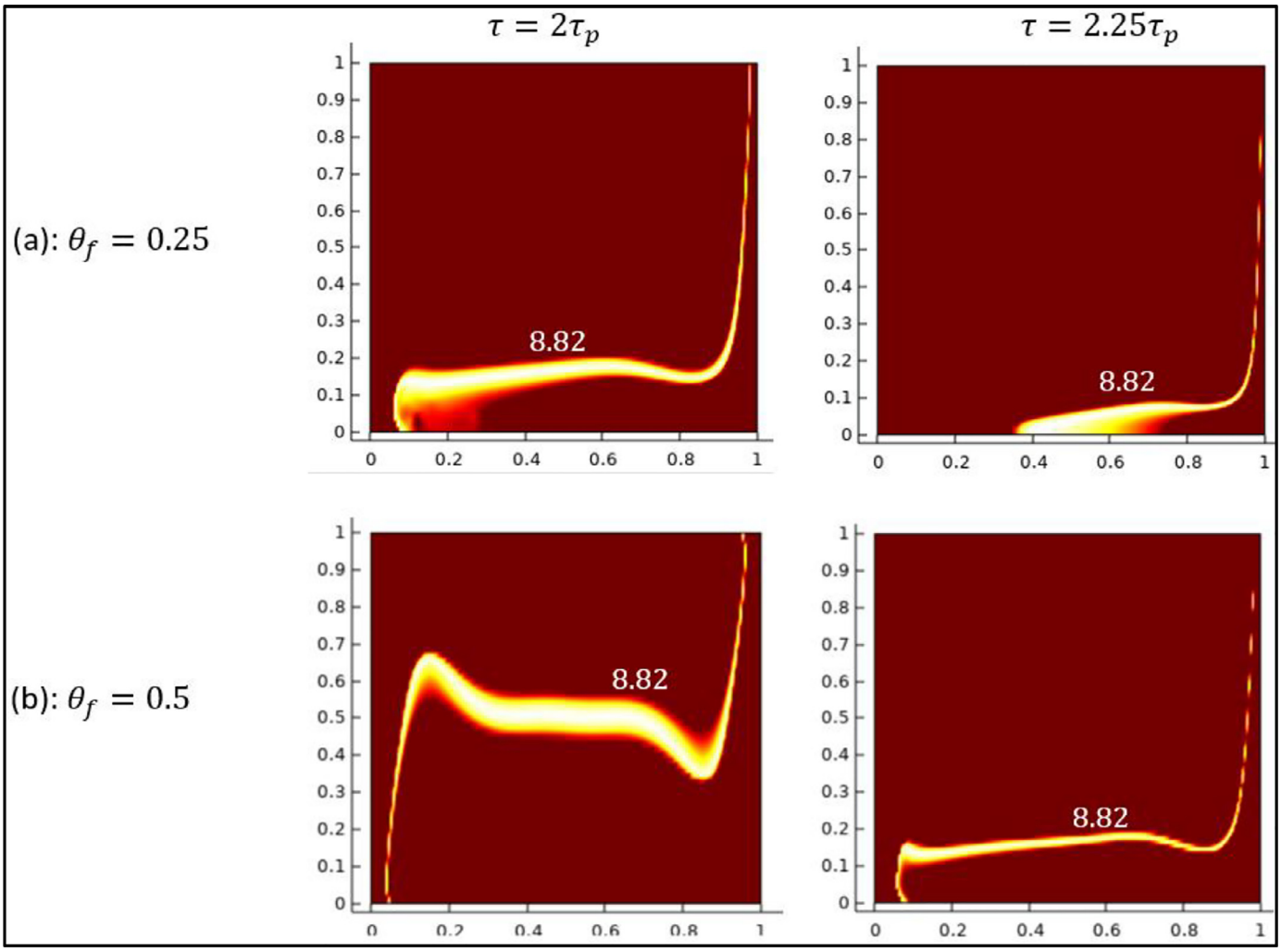

Fig. 14. Heat capacity ratio *Cr* contours for $\theta_f = 0.25$ and $\theta_f = 0.5$.

heat released and absorbed during the phase change by the NEPCM is included in the equations. The governing equations are solved by means of the finite element method with adequate boundary conditions. The main parameter that is measured to assess heat transfer inside the cavity is the average Nusselt number $Nu_{a,\tau}$, of which the variation is tracked as a function of time. Various values of the dimensionless parameters affecting the flow and heat transfer behaviors in the cavity are considered. The main results of the study can be summarized as follows:

In the case of time-periodic temperature boundary condition, the Nusselt number $Nu_{a,\tau}$ follows the variation of the temperature. $Nu_{a,\tau}$ varies periodically around an average value Nu_a and has the same frequency as the temperature. An increase in the amplitude of the temperature increases the amplitude of $Nu_{a,\tau}$, but the average Nu_a remains the same. Nu_a represents the value of Nusselt number in the case of a constant temperature boundary condition, i.e., when the amplitude of the temperature is zero.

Using a higher volume fraction ϕ of the NEPCM particles increases the Normalized average Nusselt number $NNu_{\phi=0}$ and the amplitude of $Nu_{a,\tau}$, and, thus, enhances heat transfer in the enclosure. The optimal value of ϕ is 0.05, which improves heat transfer while respecting the condition of dilute suspension. *Ra* is another parameter which when increased, enhances heat transfer by increasing Nu_a.

Increasing the latent heat of the PCM core of the NEPCM particles (by decreasing the value of Stefan number *Ste*) further enhances heat transfer in the cavity by increasing the values of $Nu_{a,\tau}$ under the same temperature conditions. Varying the fusion temperature of the PCM core also affects heat transfer. In fact, using fusion temperature close to the temperature of the cold wall or to the maximum temperature θ_{max} of the hot wall reduces the heat transfer. The heat transfer is optimal when the fusion temperature is in the range $[0.25\ \theta_{max}, 0.75\theta_{max}]$.

In the present study, the heat transfer and fluid flow of a cavity with a constant and time-periodic wall temperature are investigated. The Nusselt number is investigated as the charasterestic parameter for wall temperature. There are many applications that the cavity is subject to a constant or variable heat flux instead of constant wall temperature. As the nanocapsules contribute to temperature control of the cavity by their latent heat, the investigation of the effect of nano-capsulses on the temperature distribution of a cavity wall subject to a constant or variable wall heat flux can be investigated in future studies.

Declaration of Competing Interest

The authors clarify that there is no conflict of interest for report.

References

[1] Keshteli AN, Sheikholeslami M. Nanoparticle enhanced pcm applications for intensification of thermal performance in building: a review. J Mol Liq 2018;274:516–33.
[2] Moreno P, Solé C, Castell A, Cabeza LF. The use of phase change materials in domestic heat pump and air-conditioning systems for short term storage: a review. Renewable Sustainable Energy Rev 2014;39:1–13.
[3] Pielichowska K, Pielichowski K. Phase change materials for thermal energy storage. Prog Mater Sci 2014;65:67–123.

[4] Sheikholeslami M. Numerical modeling of nano enhanced pcm solidification in an enclosure with metallic fin. J Mol Liq 2018;259:424–38.
[5] Bondareva N, Sheremet M. Natural convection melting of nano-enhanced phase change material in a cavity with finned copper profile. MATEC Web of Conferences. EDP Sciences; 2018.
[6] Hossain R, Mahmud S, Dutta A, Pop I. Energy storage system based on nanoparticle-enhanced phase change material inside porous medium. Int J Therm Sci 2015;91:49–58.
[7] Lin Y, Jia Y, Alva G, Fang G. Review on thermal conductivity enhancement, thermal properties and applications of phase change materials in thermal energy storage. Renewable Sustainable Energy Rev 2018;82:2730–42.
[8] Qureshi ZA, Ali HM, Khushnood S. Recent advances on thermal conductivity enhancement of phase change materials for energy storage system: a review. Int J Heat Mass Transf 2018;127:838–56.
[9] Chai L, Shaukat R, Wang L, Wang HS. A review on heat transfer and hydrodynamic characteristics of nano/microencapsulated phase change slurry (N/MPCS) in mini/microchannel heat sinks. Appl Therm Eng 2018;135:334–49.
[10] Fang G, Li H, Yang F, Liu X, Wu S. Preparation and characterization of nano-encapsulated n-tetradecane as phase change material for thermal energy storage. Chem Eng J 2009;153:217–21.
[11] Qiu X, Li W, Song G, Chu X, Tang G. Fabrication and characterization of microencapsulated n-octadecane with different crosslinked methylmethacrylate-based polymer shells. Sol Energy Mater Sol Cells 2012;98:283–93.
[12] Jamekhorshid A, Sadrameli S, Farid M. A review of microencapsulation methods of phase change materials (PCMs) as a thermal energy storage (TES) medium. Renewable Sustainable Energy Rev 2014;31:531–42.
[13] Su W, Darkwa J, Kokogiannakis G. Review of solid–liquid phase change materials and their encapsulation technologies. Renew. Sustain. Eng Rev 2015;48:373–91.
[14] Ghalambaz M, Doostani A, Izadpanahi E, Chamkha A. Phase-change heat transfer in a cavity heated from below: the effect of utilizing single or hybrid nanoparticles as additives. J Taiwan Inst Chem Eng 2017;72:104–15.
[15] Hosseini S, Sheikholeslami M, Ghasemian M, Ganji D. Nanofluid heat transfer analysis in a microchannel heat sink (MCHS) under the effect of magnetic field by means of kkl model. Powder Technol 2018;324:36–47.
[16] Sheikholeslami M, Sadoughi M. Simulation of cuo-water nanofluid heat transfer enhancement in presence of melting surface. Int J Heat Mass Transf 2018;116:909–19.
[17] Chamkha A, Doostanidezfuli A, Izadpanahi E, Ghalambaz M. Phase-change heat transfer of single/hybrid nanoparticles-enhanced phase-change materials over a heated horizontal cylinder confined in a square cavity. Adv Powder Technol 2017;28:385–97.
[18] Elbahjaoui R, El Qarnia H. Transient behavior analysis of the melting of nanoparticle-enhanced phase change material inside a rectangular latent heat storage unit. Appl Therm Eng 2017;112:720–38.
[19] Alsabery AI, Mohebbi R, Chamkha AJ, Hashim I. Effect of local thermal non-equilibrium model on natural convection in a nanofluid-filled wavy-walled porous cavity containing inner solid cylinder. Chem Eng Sci 2019;201:247–63.
[20] Hashim I, Alsabery A, Sheremet M, Chamkha A. Numerical investigation of natural convection of Al_2O_3-water nanofluid in a wavy cavity with conductive inner block using Buongiorno's two-phase model. Adv Powder Technol 2019;30:399–414.
[21] Sivaraj C, Sheremet M. MHD natural convection and entropy generation of ferrofluids in a cavity with a non-uniformly heated horizontal plate. Int J Mech Sci 2018;149:326–37.
[22] Ghalambaz M, Sheremet MA, Mehryan S, Kashkooli FM, Pop I. Local thermal non-equilibrium analysis of conjugate free convection within a porous enclosure occupied with Ag–MgO hybrid nanofluid. J Therm Anal Calorim 2019;135:1381–98.
[23] Tahmasebi A, Mahdavi M, Ghalambaz M. Local thermal nonequilibrium conjugate natural convection heat transfer of nanofluids in a cavity partially filled with porous media using Buongiorno's model. Numer Heat Transfer, Part A 2018;73:254–76.
[24] Alsabery AI, Armaghani T, Chamkha AJ, Sadiq MA, Hashim I. Effects of two-phase nanofluid model on convection in a double lid-driven cavity in the presence of a magnetic field. Int. J. Numer Methods for Heat & Fluid Flow 2019;29:1272–99.
[25] Alsabery AI, Tayebi T, Chamkha AJ, Hashim I. Effects of two-phase nanofluid model on natural convection in a square cavity in the presence of an adiabatic inner block and magnetic field. Int. J. Numerical Methods for Heat & Fluid Flow 2018;28:1613–47.
[26] Seyf HR, Zhou Z, Ma H, Zhang Y. Three dimensional numerical study of heat-transfer enhancement by nano-encapsulated phase change material slurry in microtube heat sinks with tangential impingement. Int J Heat Mass Transf 2013;56:561–73.
[27] Seyf HR, Wilson MR, Zhang Y, Ma H. Flow and heat transfer of nanoencapsulated phase change material slurry past a unconfined square cylinder. J Heat Transfer 2014;136:051902.
[28] Ho C-J, Chen W-C, Yan W-M. Experimental study on cooling performance of minichannel heat sink using water-based MEPCM particles. Int Commun Heat Mass Transf 2013;48:67–72.
[29] Ho C-J, Huang J, Tsai P, Yang YM. Water-based suspensions of Al_2O_3 nanoparticles and MEPCM particles on convection effectiveness in a circular tube. Int J Therm Sci 2011;50:736–48.
[30] Ho C-J, Chen W-C, Yan W-M. Correlations of heat transfer effectiveness in a minichannel heat sink with water-based suspensions of Al_2O_3 nanoparticles and/or MEPCM particles. Int J Heat Mass Transf 2014;69:293–9.
[31] Ghalambaz M, Chamkha AJ, Wen D. Natural convective flow and heat transfer of nano-encapsulated phase change materials (NEPCMs) in a cavity. Int J Heat Mass Transf 2019;138:738–49.
[32] Barlak S, Sara ON, Karaipekli A, Yapıcı S. Thermal conductivity and viscosity of nanofluids having nanoencapsulated phase change material. Nanoscale Microscale Thermophys Eng 2016;20:85–96.
[33] Ghalambaz M, Sheremet MA, Pop I. Free convection in a parallelogrammic porous cavity filled with a nanofluid using Tiwari and Das' nanofluid model. PLoS One 2015;10:e0126486.
[34] Chen B, Wang X, Zeng R, Zhang Y, Wang X, Niu J, Li Y, Di H. An experimental study of convective heat transfer with microencapsulated phase change material suspension: laminar flow in a circular tube under constant heat flux. Exp Therm Fluid Sci 2008;32:1638–46.
[35] Khanafer K, Vafai K. A critical synthesis of thermophysical characteristics of nanofluids. Int J Heat Mass Transf 2011;54:4410–28.
[36] Zaraki A, Ghalambaz M, Chamkha AJ, Ghalambaz M, De Rossi D. Theoretical analysis of natural convection boundary layer heat and mass transfer of nanofluids: effects of size, shape and type of nanoparticles, type of base fluid and working temperature. Adv Powder Technol 2015;26:935–46.
[37] Zienkiewicz OC, Taylor RL, Nithiarasu P. The finite element method for fluid dynamics. In: The finite element method for fluid dynamics. Oxford: Butterworth-Heinemann; 2014. pp. iii.
[38] De Los Reyes JC, González Andrade S. A combined BDF–semismooth newton approach for time–dependent bingham flow. Numer Methods Partial Differ Equ 2012;28:834–60.
[39] Turan O, Sachdeva A, Chakraborty N, Poole RJ. Laminar natural convection of power-law fluids in a square enclosure with differentially heated side walls subjected to constant temperatures. J Nonnewton Fluid Mech 2011;166:1049–63.
[40] Kahveci K. Buoyancy driven heat transfer of nanofluids in a tilted enclosure. J Heat Transfer 2010;132:062501.
[41] Kalabin EV, Kanashina MV, Zubkov PT. NATURAL-CONVECTIVE heat transfer in a square cavity with time-varying side-wall temperature. Numerical Heat Transfer, Part A: Applications 2005;47:621–31.